Fatigue Damage Development in 14MoV6-3 Steel for Power Plant Pipes Monitored by Digital Image Correlation

M. Kopec[1,2]

Abstract

In this paper, fatigue damage development of 14MoV6-3 (13HMF) power engineering steel was studied through different experimental and analytical approaches. The specimens machined from the as-received pipe were subjected to fatigue loading and simultaneously monitored using the digital image correlation (DIC) technique. The damage development was analysed through microstructural observations of fracture surfaces and further described as a function of the fatigue damage parameter D and the fatigue damage measure ϕ. The combination of such parameters' evolution with the number of cycles to failure and the DIC technique enables a determination of separate stages of damage development. It was found that dynamics of damage could be effectively exposed within the first 100 cycles.

Keywords Fatigue development · Damage · 13HMF steel · Digital image correlation (DIC)

1 Introduction

Power engineering steels are a group of construction alloy steels dedicated to pressure components working at an elevated temperature [1]. Among them, 13HMF chromium-molybdenum-vanadium steel is used in the production of boiler tubes, parts of steam turbines and boilers working at temperature up to 560 °C [2]. The degradation of such components occurs, among others, due to complex loading conditions under which they are operating. These accelerate the development of damage dynamics significantly and therefore the monitoring of power engineering steel pipes subjected to continuous operations remains a critical issue to maintain their safe state and subsequently minimize the operating costs of industrial structures [3]. Conventional techniques that enable the determination of mechanical parameters under various loading types such as fatigue include extensometer and tensometer recordings.

These methods both allow for continuous registration of strain changes during the test. However, they only effectively monitor a limited strain gauge of the specimen, and more importantly, provide average data from such measurements [4]. Such serious limitation in terms of fatigue testing remains a crucial issue since the crack prediction, its localisation and subsequent damage development are of local nature. It should be highlighted that accurate prediction and subsequent localisation of the crack initiation within the gauge length are practically impossible using conventional extensometers or tensometers, thus material models [5, 6] and finite element simulations [7] are widely used for such purpose. Such a problem may be effectively solved by the application of full-field optical methods that enable measurement of fatigue crack closure [8], as well as residual stress determination [9], or optical stress concentration and stress gradient monitoring [10]. Risbet et al. [11] proposed an application of digital image correlation (DIC) in early fatigue damage detection in stainless steel under a low-cycle regime for the purpose of developing a numerical model that can further enable accurate prediction of the fatigue life of a structural component. Furthermore, Qvale et al. [12] elaborated a DIC-based technique for continuous mapping of fatigue crack initiation sites on the corroded surface from offshore mooring chain which enables successful determination of multiple initiation sites on a single surface. Vanlanduit et al. [13] used DIC assisted by stroboscopic illumination to monitor the crack growth

✉ M. Kopec
  mkopec@ippt.pan.pl; m.kopec16@imperial.ac.uk

1   Institute of Fundamental Technological Research Polish Academy of Sciences, 5b Pawińskiego Str, 02-106 Warsaw, Poland

2   Department of Mechanical Engineering, Imperial College London, London SW7 2AZ, UK

process during a cyclic fatigue test, in which 8100 images of the crack propagation process were recorded. Niendorf et al. [14] successfully utilised the suitability of the DIC technique for monitoring fatigue-induced damage evolution in ultrafine-grained interstitial-free steel within the low-cycle fatigue regime. The authors have confirmed that the crack initiation area could be effectively detected using DIC at the very early stages of cyclic deformation by capturing the localized high strains which accumulate and subsequently cause the nucleation of surface cracks. El Bartali et al. [15] used DIC on the micro-structural scale to understand and obtain quantitative values of the fatigue surface damage in duplex stainless steel under a low-cycle fatigue regime. Since the fatigue damage mechanisms were successfully revealed after testing, it was concluded that strain field measurements are a good tool for studying the behaviour of metals under fatigue damage, especially in regard to strain gradients which are forewarning signs of microcrack initiation. Koster et al. [16] used DIC for the characterization of fatigue damage evolution in brazed steel joints. In this research, DIC was applied to determine the strain distribution in the vicinity of the brazed layer before a fracture occurs. The authors highlighted that further experiments with simultaneous DIC and extensometer measurements should be performed to quantify the strain accumulation due to cyclic loading on the one hand, and to achieve a better understanding of the failure mechanisms on the other. Tanvir et al. [17] presented an attempt to identify the fatigue damage evolution in 316L stainless steel using acoustic emission (AE), DIC and Renyi's entropy. Renyi's entropy was defined as a quantitative parameter that measures the uncertainty or randomness of the signals. Its validity was investigated by performing AE monitoring during fatigue testing of 316L stainless steel supported by DIC. In such research, global strain monitoring by DIC was performed to relate material damage with AE activity. It was found that Renyi's entropy is an effective measure to identify critical stages of damage in the material.

One should highlight that quantitative parameters that could define or describe fatigue damage monitoring are still in the interest of the mechanical engineering field since they could be effectively used to describe the changes within material integrity during fatigue performance, especially in a high-cycle regime. Since the conventional S–N curves only represent the magnitudes of stress amplitude as a function of the number of cycles to fracture without providing any knowledge on fatigue damage mechanisms that occurred during testing, the proposed methodology of damage parameters could be effectively used to analyse the fatigue behaviour in the whole range of testing, from the very first to the last loading cycle, thus reflecting the physical mechanisms of damage evolution. This paper aims to propose an effective methodol-ogy to assess the dynamics of fatigue damage development in 13HMF steel subjected to fatigue loading with the additional support of the DIC technique. The quantitative assessment of the degradation state in such power engineering steel was described as a function of the fatigue damage measure ϕ and the fatigue damage parameter D, and further combined with the DIC method to reveal the dynamics of fatigue damage development depending on the stress applied.

2 Materials and Methods

2.1 Material Characterization

The material was supplied in the form of a half-meter-long pipe in the as-received state (normalization at 940–960 °C, and 700–730 °C during tempering) [18]. The chemical composition of the material confirmed the agreement with the Polish Standards (PN-75/H-84024) [18] as presented in Table 1.

2.2 Experimental Details

At the beginning of the experimental procedure, specimens were machined from the pipe section as presented in Fig. 1a. The geometry of the specimen is shown in Fig. 1b. Subsequently, standard tensile tests at the strain rate equal to 2×10^{-4} s^{-1} were performed to assess the mechanical properties of 13HMF steel. Based on these test results, fatigue loading conditions were determined. Both uniaxial tensile and fatigue tests were performed by using a conventional MTS 858 testing machine (Fig. 1c). The fatigue tests were force-controlled with $(\sigma_{max} - \sigma_{min})/2$ level and a stress asymmetry coefficient $R = 0$ with a frequency of 20 Hz in the stress range $(\Delta\sigma)$ from 320 to 500 MPa. Three specimens per condition were used to guarantee the reliability of the results obtained. Before and during fatigue tests, the specimens were pre-stretched to the stress value equal to $+ 10$ MPa in order to avoid buckling. The strain values in the description of the hysteresis loop were recorded by the conventional MTS extensometer with a gauge length of 25 mm. Simultaneously, the strain distribution on the specimen surface was monitored during fatigue tests by using DIC Aramis 12 M equipped with lenses of a total focal length of 75 mm and calibration settings appropriate to the measuring area equal to 170 mm × 156 mm. The calibration was performed prior to testing using a certified GOM calibration plate. Aramis software was used to capture DIC images automatically at σ_{max} each 1000 fatigue cycles.

Table 1 Chemical composition of 13HMF steel in as-received condition and according to the Polish Standards PN-75/H-84024 [18]

	C	Si	Mn	P	S	Cr	Mo	Ni	Fe
As-received state	0.15	0.30	0.60	0.02	0.02	0.55	0.55	0.25	Bal
PN-75/H-84024	0.1–0.18	0.15–0.35	0.4–0.7	< 0.04	< 0.04	0.3–0.6	0.5–0.65	< 0.3	Bal

(a)

(b)

(c)
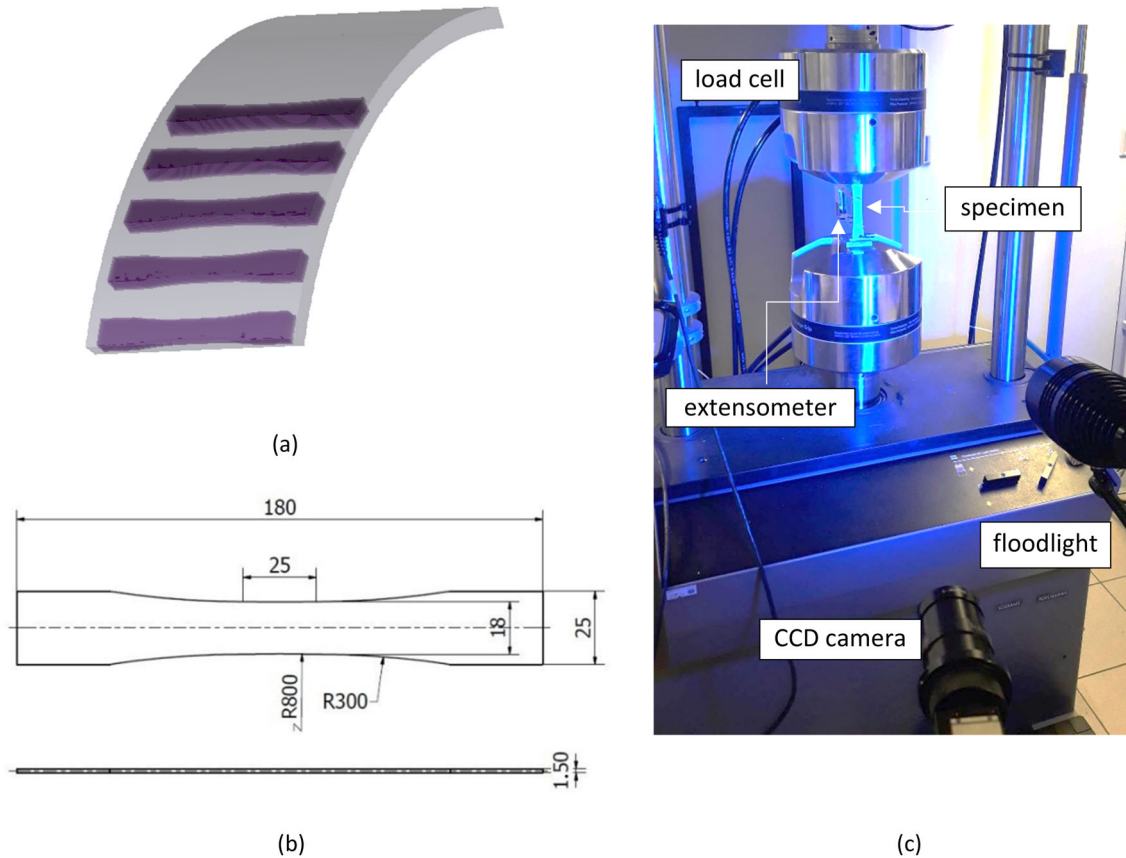
Fig. 1 **a** Distribution of specimens for mechanical testing in a pipe section; **b** specimen geometry; **c** general view of the experimental setup: DIC and MTS testing machine

3 Results and Discussion

3.1 Mechanical Properties of 13HMF Steel

Selected mechanical properties of 13HMF steel were obtained from static tensile tests during which the yield point, ultimate tensile strength and elongation were determined (Fig. 2a, Table 2). The reliability of the results was further confirmed by testing five specimens accordingly. It was found that the supplied material meets the requirements of the PN-75/H-84024 [18] standard regarding its mechanical properties. Subsequently, fatigue tests with different values of stress ranging from 320 to 500 MPa were carried out as shown in Table 3 and Fig. 2b, where the *S–N* curve that summarises the fatigue results obtained is presented. The confidence intervals obtained for each stress

Table 2 Mechanical parameters of 13HMF steel in as-received condition and according to the Standards PN-75/H-84024 [18]

	Ultimate tensile strength (MPa)	Yield strength (MPa)	Elongation (%)
As-received state	615($\pm$ 2)	355($\pm$ 4)	26($\pm$ 1)
PN-75/H-84024	460–610	> 300	> 20%

condition were approximately equal to 15%, which further confirmed the repeatability of the fatigue tests performed. One should notice a significant increase in the service life for the specimens subjected to cyclic loading at a stress lower than 480 MPa. On the other hand, the fatigue stress amplitude limit representing stress amplitude enabling to carry 10^7
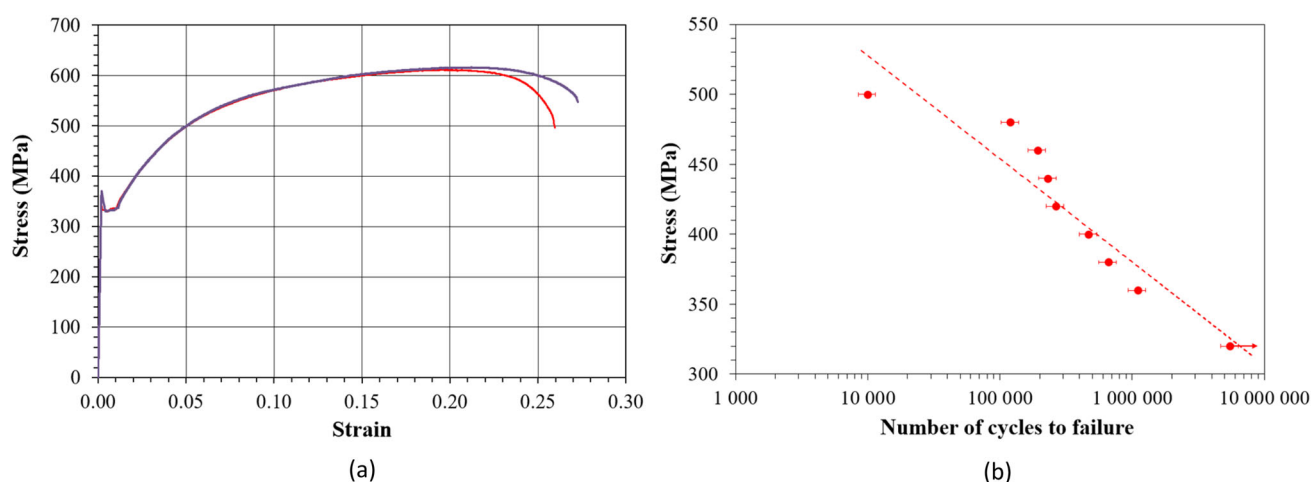
Fig. 2 Representative tensile curve: **a** and *S–N* curve: **b** for 13HMF steel in as-received condition

loading cycles according to the Polish Standards [19] was assumed to be equal to 320 MPa. Since the extensometer did not record any strain changes in the following cycles, the test at such specific stress was interrupted after reaching 8.5×10^6 cycles.

3.2 Fatigue Damage Development in 13HMF Steel Monitored by Digital Image Correlation

Fatigue damage is the progressive, localized, and permanent structural change that occurs in a material subjected to repeated or fluctuating strains [20]. It is characterized by the nucleation, coalescence, and stable growth of cracks that ultimately lead to net section yielding or brittle fracture [21]. In order to effectively monitor its development in 13 HMF steel, a full-field optical method was used to record the changes in strain distribution on the specimen surface after a specific number of cycles. Since the testing machine was coupled with the DIC measurement setup, a special testing programme was developed to automatically enforce the image recording, when the stroke of the testing machine would register the extension of the specimen by 0.5 mm. Furthermore, the specimen's geometry enabled localisation of the potential crack initiation to the area with the smallest cross-section located on the edge of the specimen. It was observed that the crack initiation area was indeed found in the central part of specimens subjected to cyclic loading in the wide range of stress (Fig. 3). It should be noticed that increased values of strain in the central part of specimens were found after just one cycle.

The subsequent damage development progresses with the following cycles, however, the area of potential crack initiation could be distinguished when the specimen reached approximately one-third of its service life. Such a phenomenon could be observed for all specimens regardless of the stress value applied (Fig. 3a–c). One should mention that more inhibited fatigue damage development could be observed for the specimens subjected to lower stress (Fig. 3a). Even though the crack propagation area was clearly observed after 600 000 cycles, the specimen was able to transfer ~ 60000 more cycles before its failure. With an increase in the stress, less pronounced effects were observed, however, they were still proportional to the service life of the specimen subjected to the specific stress and further expressed by the number of cycles to failure (Fig. 3b, c).

One should highlight that the effect of stress on fatigue damage mechanisms in power engineering steels is mainly driven by the interaction of inclusions with a material matrix, thus the fractographic analysis would be crucial to revealing deformation mechanisms.

3.3 Microscopic Analysis of Damage Development in 13HMF Steel

The microscopic observations performed near the fatigue crack source area for all specimens revealed a ductile fracture consisting of fine dimples distributed evenly on the surface. It should be emphasised that the specimen subjected to a stress of 380 MPa possesses a coarser surface with large craters with some inclusions and areas of microvoids located inside

Table 3 The number of cycles to failure in relation to the stress applied

Stress (MPa)	500	480	460	440	420	400	380	360	320
Number of cycles to failure	9969	119853	192350	230722	264218	468617	658647	1100536	8500000
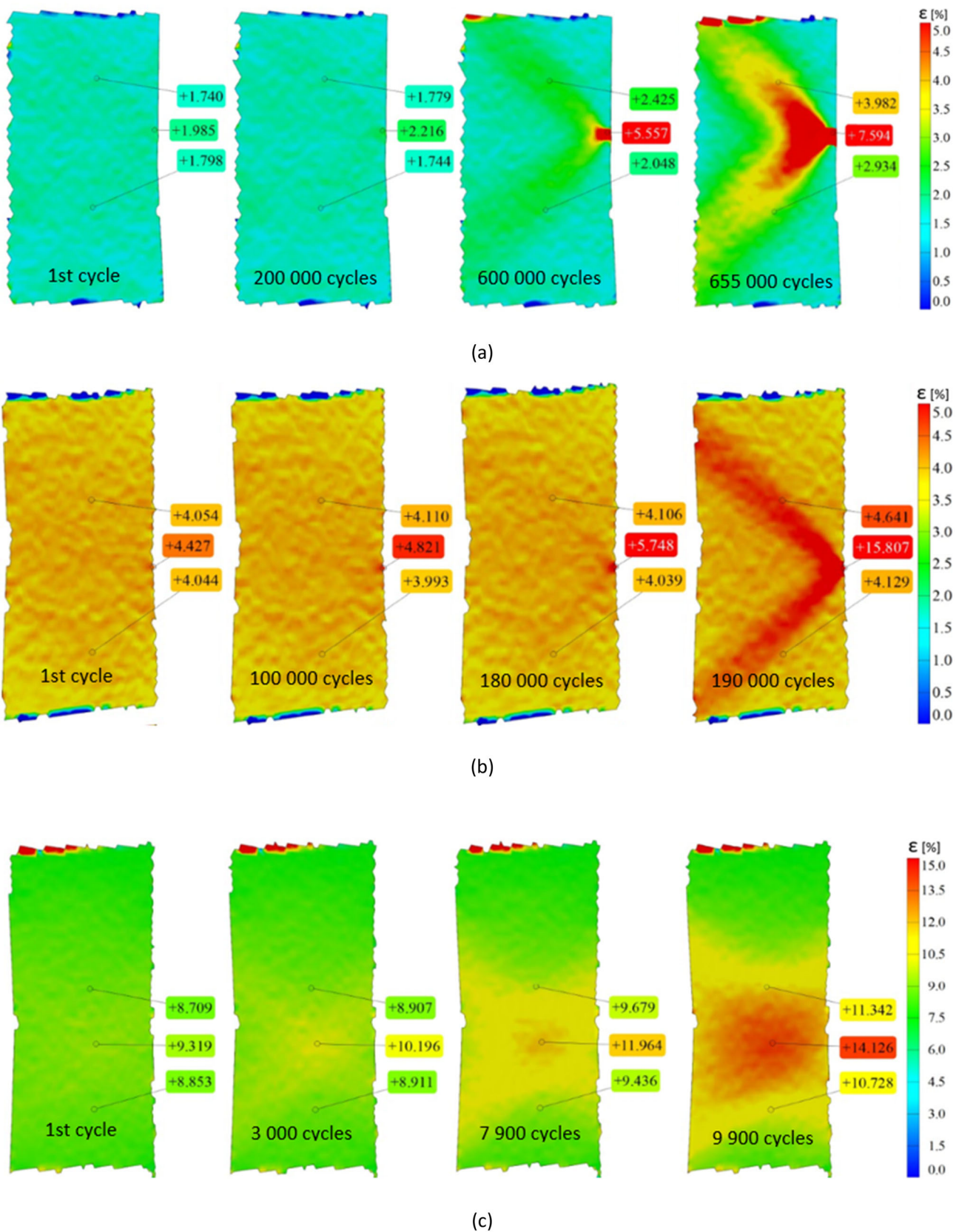
Fig. 3 Selected DIC measurements for the specimens subjected to fatigue testing at stress equal to **a** 380 MPa; **b** 460 MPa; and **c** 500 MPa
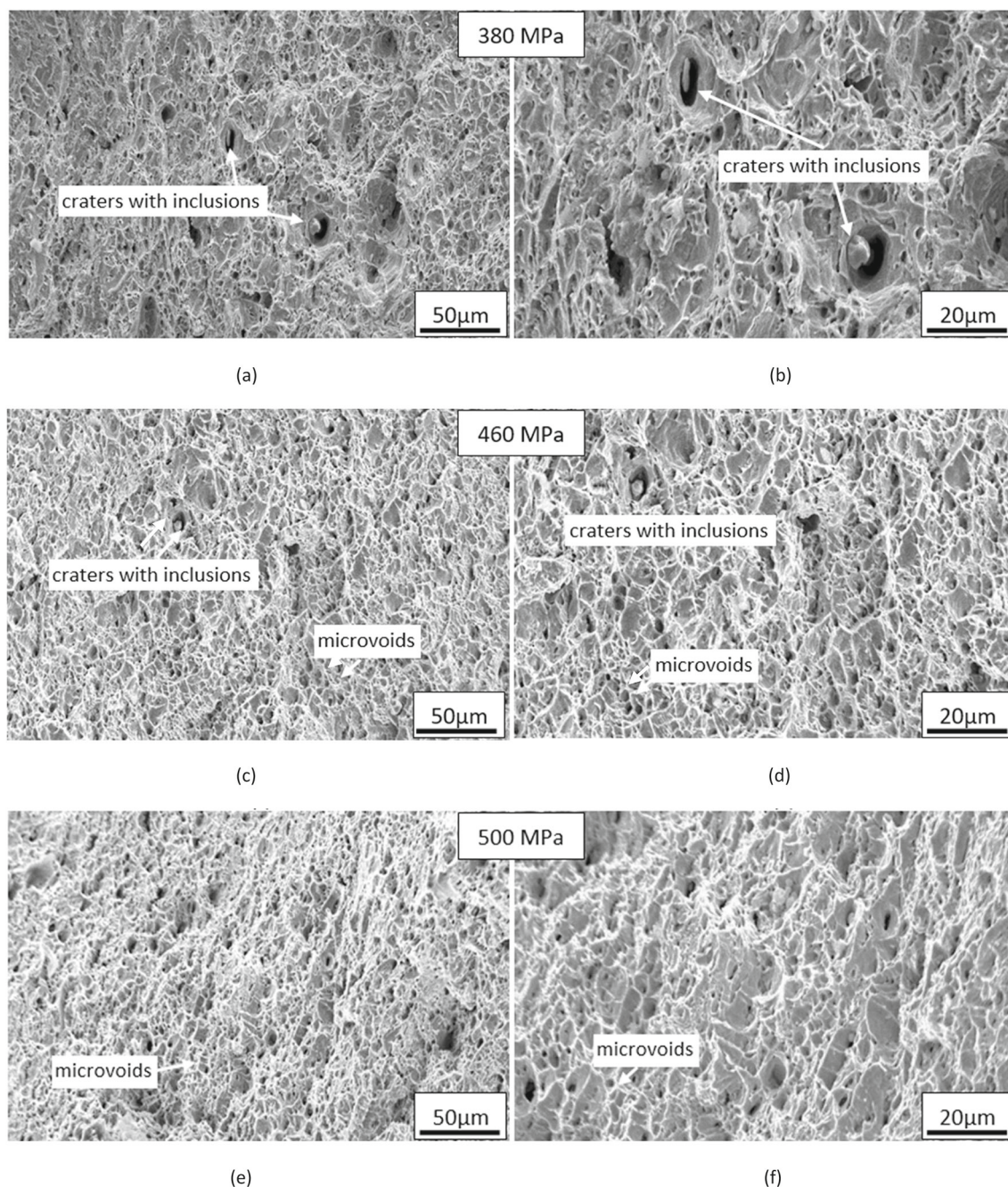
Fig. 4 The fracture area of the specimens after being subjected to the fatigue test at the stress of **a-b** 380 MPa; **c-d** 460 MPa; and **e–f** 500 MPa

or around them (Fig. 4a, b). The regular shape of these craters is possibly related to the fact that the decoherence processes observed under cyclic loading were initiated by inclusions, which were located in craters larger than their actual size (Fig. 4b). Thus it could be claimed that the plastic strain propagation nucleates near inclusions which serve as stress concentrators [22]. On the other hand, the presence of smaller microvoids in the surrounding areas near inclusions results

from fatigue interaction between hard and brittle inclusions and metal matrix [23].

One should highlight that the decrease in stress results in an increase in the size of the craters and dimples. It could be observed that the specimen subjected to a stress of 380 MPa possesses craters approximately 20 μm wide, which are not much larger than the inclusions found inside them (Fig. 4b). On the contrary, those tested at 460 MPa and 500 MPa are characterized by the fracture surface covered mostly by fine

dimples (Fig. 4d, f). The inclusions found in the craters have almost the same size. Such a phenomenon is also related to fatigue interaction between inclusions and matrix. The lower is the stress, the longer interaction time is applied and thus more prominent microstructural changes could be observed. The damage development mechanisms of metallic materials operating in high-cycle regime could be divided into two basic types: cyclic plasticity and ratcheting. The cyclic plasticity is generated by micro-slips and the subsequent formation of slip bands. Microstructure changes mainly involve multiplication and rearrangement of dislocations [23]. On the other hand, the fracture surface of specimens subjected to fatigue loading that further exhibits the ratcheting effect is characterized by a ductile fracture with local deformations around voids and non-metallic inclusions [24]. Such features were observed in Fig. 4 regardless of the stress used, thus it was concluded that the main mechanism responsible for fatigue damage development in 13HMF steel is ratcheting.

The correlation of DIC measurements and microscopic observations enabled to reveal different damage mechanisms in relation to the stress applied. It could be observed that the 13HMF steel specimen subjected to the stress of 380 MPa exhibited strain concentration and further crack initiation on the right edge of the middle section of the gauge (Fig. 3a, Fig. 5a). The SEM observations performed on such an area exposed a crack source area, which propagated from the specimen edge. Furthermore, some inclusions found in the crack tip acted as stress concentrators and accelerated the damage process during fatigue.

On the other hand, the specimen subjected to fatigue testing under the stress of 500 MPa exhibited a strain accumulation area in the central area of the gauge (Figs. 3c and 5b), and in such a region, the fracture occurred. The observations performed in the middle section (area II) revealed the strong interaction of inclusion with the matrix since the large area of fine dimples was found below the non-metallic particle (Fig. 5b). The crack propagated towards the specimen edges, where the material was still coherent. The excessive stress acting on the specimen's external areas led to the formation of microvoids in the plastically deformed edges. Although the fracture mechanism of each specimen is different, both of them exhibited the same classical phenomena involving cyclic plastic deformation till the initiation of one or more microcracks, coalescence of microcracks, and formation of one or more macroscopic cracks that subsequently propagate, causing material fracture [25]. Such behaviour is, however, more prominent for the specimen subjected to the fatigue testing at 380 MPa, where all stages, from micro to macro scale, could be observed by using SEM and DIC, respectively (Fig. 5a). The area of fatigue crack initiation was also located near singularities (inclusion, embrittled grain boundaries, sharp scratches) just below the surface and on the edge of the specimen, where the stress concentration occurred. On the contrary, during the fatigue testing at 500 MPa, a significant plastic deformation was introduced to the central region of the strain gauge (Fig. 5b). The crack initiated in area II, where many inclusions acting as stress concentrators were found. Once the macrocrack occurred in the middle section of the specimen, its propagation was temporarily inhibited on the edges of the specimens, where microvoids formed due to excessive stress applied.

3.4 Quantitative Assessment of the Fatigue Damage Development in 13HMF Steel

The mechanical response registered for 13HMF steel and presented in the form of *S–N* curve is the conventional approach to determine the service life of the material. However, the determination of the typical *S–N* curve is costly and time-consuming [26]. The physically-based alternative method presented by the author [25, 27] includes the evolution of deformation dynamics development due to the ratcheting and cyclic plasticity registered in subsequent cycles for the range of stress applied (Fig. 6a). These changes were subsequently parametrized and described as the fatigue damage measure ϕ and the fatigue damage parameter *D*. The fatigue damage parameter *D* describes the dynamics of deformation changes in subsequent cycles and is represented by the relationship:

$$D = \frac{\phi_N - \phi_{\min}}{\phi_{\max} - \phi_{\min}} \tag{1}$$

where ϕ_N is the current value of the fatigue damage development measure in cycle *N*; $\phi_{\min}$ is the minimum value of the fatigue damage development measure at the beginning of the cyclic loading, i.e., for cycle $N = 1, \phi$; and $\phi_{\max}$ is the maximum value of the fatigue damage development measure for the last cycle of the period of stable damage development N_f.

In this equation, damage measure is defined by:

$$\phi = \varepsilon_w + \varepsilon_m \tag{2}$$

where ε_w is the inelastic strain amplitude being damage indicator that characterizes a width of the hysteresis loop at the total unloading; and ε_m is the mean inelastic strain responsible for a shift of the hysteresis loop under unloaded state.

The inelastic strain amplitude was measured at the total unloading of a material and described in a single cycle by:

$$\varepsilon_w = \frac{\varepsilon_{\max}^{\sigma=\sigma_{\max}/2} - \varepsilon_{\min}^{\sigma=\sigma_{\max}/2}}{2} \tag{3}$$
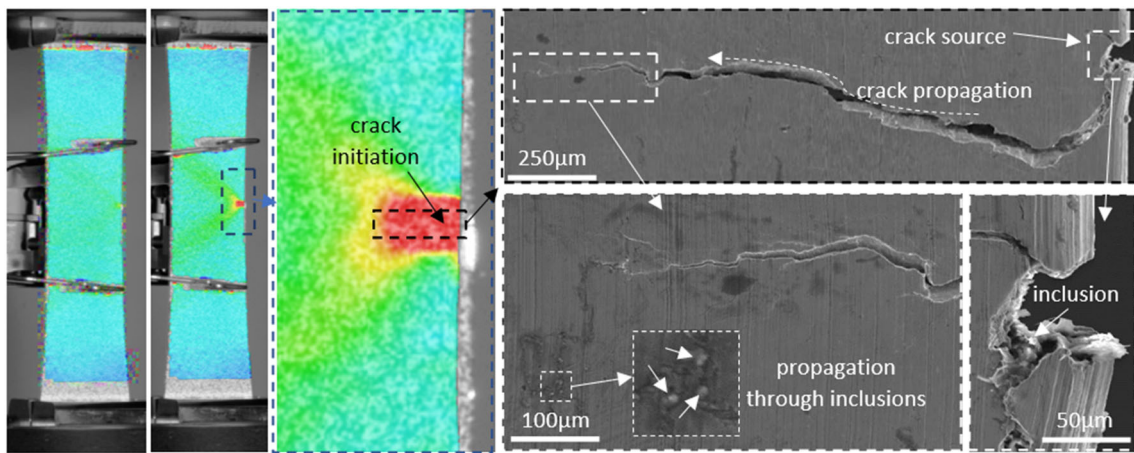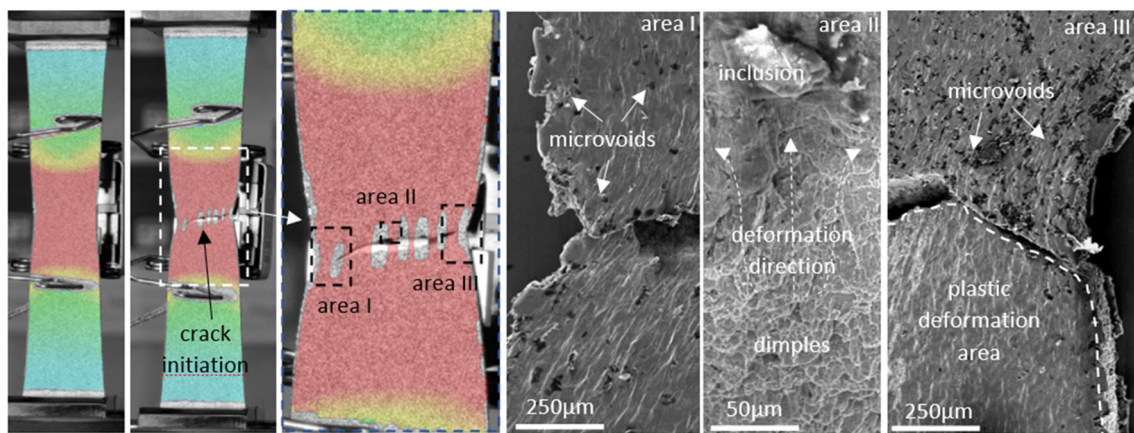
Fig. 5 Correlation of DIC measurements and SEM observations during fatigue damage development of 13HMF steel subjected to testing under pulsating loading of **a** 380 MPa; and **b** 500 MPa
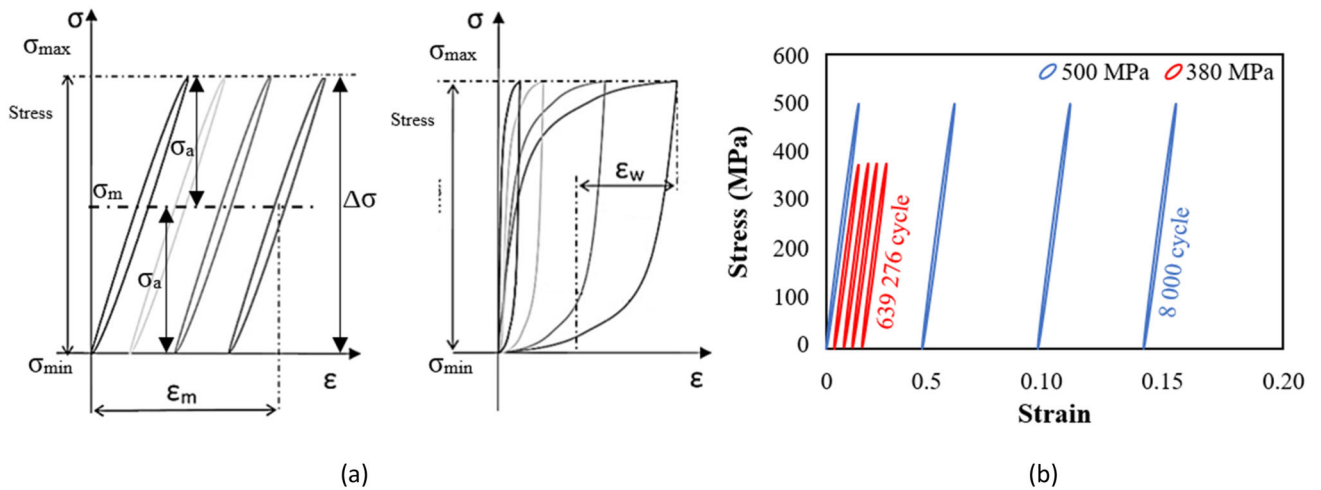
Fig. 6 a Schema of hysteresis loop evolution in subsequent fatigue cycles for 13HMF steel, where σ_m is the mean stress, σ_a is stress amplitude, σ_{max} is the maximum stress applied, σ_{min} is the minimum stress applied, and $\Delta\sigma$ is the stress range; **b** experimental representation of the hysteresis loop shift observed during testing at different values of stress

The mean inelastic strain was also captured under unloaded state and further defined by the relationship:

$$\varepsilon_{\mathrm{m}} = \frac{\varepsilon_{\min}^{\sigma=\sigma_{\max}/2} + \varepsilon_{\max}^{\sigma=\sigma_{\max}/2}}{2} \qquad (4)$$

It should be highlighted that the microstructural changes that occurred during cyclic degradation were related to particular changes in the stress–strain response [28], thus effective indicators were used to describe and quantify each deformation mechanism. On the one hand, ratcheting generated by local deformation around the voids, inclusions and other defects [29] was related to the mean inelastic strain describing a shift of the hysteresis loop under an unloaded state (ε_{m}). On the other hand, cyclic plasticity generated by dislocation movement at the level of local grains and slip bands [30] was related to the hysteresis loop width changes at the total unloading of the material (ε_{w}). The analysis of the hysteresis loop shift during fatigue testing at both stress values of 380 MPa and 500 MPa supported by the fractographic analysis (Fig. 4) also confirmed that the main deformation mechanism responsible for damage development was ratcheting. The representative hysteresis loops for the first and last cycles recorded revealed no changes in the loop width from the beginning of the test till the specimen fracture (Fig. 6b).

The representative experimental results for the specimen subjected to the stress of 480 MPa were presented for the particular cycles at different stages of damage development as shown in Fig. 7. Determination of $\varepsilon_{\max}$ and $\varepsilon_{\min}$ for each fatigue cycle enabled to calculate the inelastic strain amplitude and mean inelastic strain required for damage parameter identification. One can define three stages of fatigue damage development:

- Stage I—elastic stress–strain behaviour of the undamaged material (Fig. 7a);
- Stage II—steady ratcheting-driven damage development prior to crack initiation (Fig. 7b);
- Stage III—crack formation and propagation (Fig. 7c)

Their better visualization could be observed in Fig. 8.

The occurrence of inclusions (Fig. 4) was found favourable for microcrack nucleation and remarkably accelerating the dynamics of the damage process in the first stage of deformation (Fig. 8). One should highlight that the width of the hysteresis loop decreases with the increase of the stress applied until the stable value of approximate 0.00015 is obtained after 100 cycles. The progressing damage of the material with subsequent cycles observed in stage II was characterized by the slight changes in the hysteresis loop width on the one hand, and significant loop shift on the other (Fig. 7b). The formation of the crack and its propagation were attributed to the strength loss and subsequent increase of the

hysteresis width (Fig. 7c). It could also be clearly observed from the significant increase of each damage parameter in the third stage of damage. Such behaviour was associated with the decoherence of material due to the rapid increase of macro cracks and their subsequent propagation in the form of dominant crack created in the final stage of damage [24]. Based on the calculations performed, it was confirmed that the main deformation mechanism responsible for fatigue damage development in 13HMF steel was ratcheting mainly reflected by the shift of the hysteresis loop.

The evolution of the fatigue damage parameter/measure as a function of the number of cycles to failure supported by DIC for the stress of 380 MPa and 500 MPa is presented in Fig. 8 in the form of live images registered during the fatigue test (Fig. 8a) and processed by Aramis software (Fig. 8b). One should note that dynamics of fatigue damage development is highly stress-dependent since considerable changes in both parameters could be observed within the first 100 cycles. It should be mentioned that for relatively low strain amplitude values, the fatigue damage development progressed steadily till the plateau stage was reached. The lower is the stress, the longer plateau could be observed. Subsequently, the damage progressed steadily till the crack and final decohesion of the specimen occurred.

The DIC methodology supported by Aramis software could also represent the measurement results in the form of strain profiles along the specimen's axis of symmetry (Fig. 9). Such representation could serve as an effective indicator of damage development since the deformation on the specimen surface registered for a particular fatigue cycle clearly indicates the deformation dynamics. In this work, the main axis of symmetry was used as a reference to monitor the damage development in subsequent cycles. One should highlight that a significant increase in strain observed after 600 000 cycles for the specimen tested at the stress of 380 MPa indicates the occurrence of crack initiation. Its further propagation could be clearly observed in the following cycles when the strain value increased and the crack propagated from the edge of the specimen (Fig. 8a). On the other hand, a steady strain increase was observed for the specimen subjected to the stress equal to 500 MPa (Fig. 8b). The strain profiles obtained for two different stress values enable to conclude that for the lower values, the strain was evenly distributed on the specimen surface till crack suddenly initiated and propagated. Such localization effect was not observed for higher values of stress, for which the gradual strain increase was observed till specimen fractured.

It should be highlighted that the DIC system alone was not able to reveal the dynamics of fatigue damage within the first 100 cycles (Figs. 8 and 9). Some strain increase might be found in the central area of the specimen, however, its prominent intensification occurred in the second stage of

Fig. 7 Representative hysteresis loop evolution in particular fatigue cycles for 13HMF steel subjected to the stress equal to 480 MPa at different stages of fatigue damage development: **a** elastic stress–strain behaviour of the undamaged material; **b** steady ratcheting-driven damage development; **c** crack formation and propagation
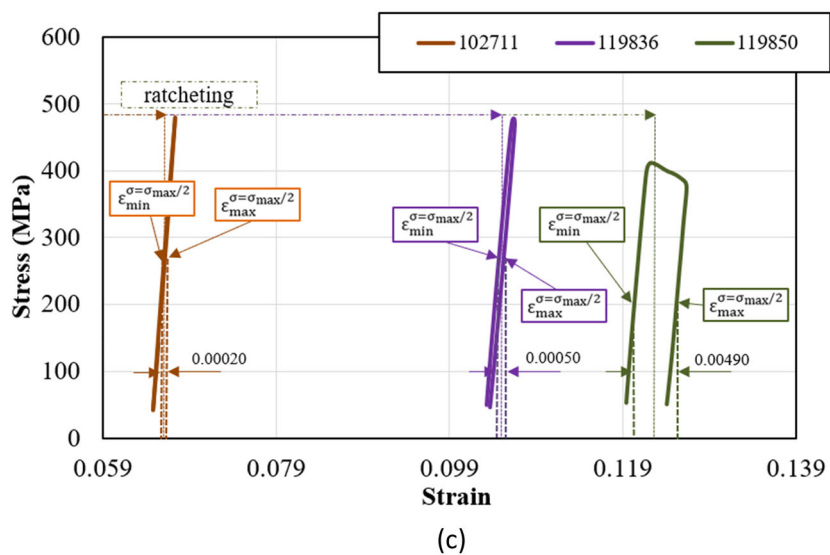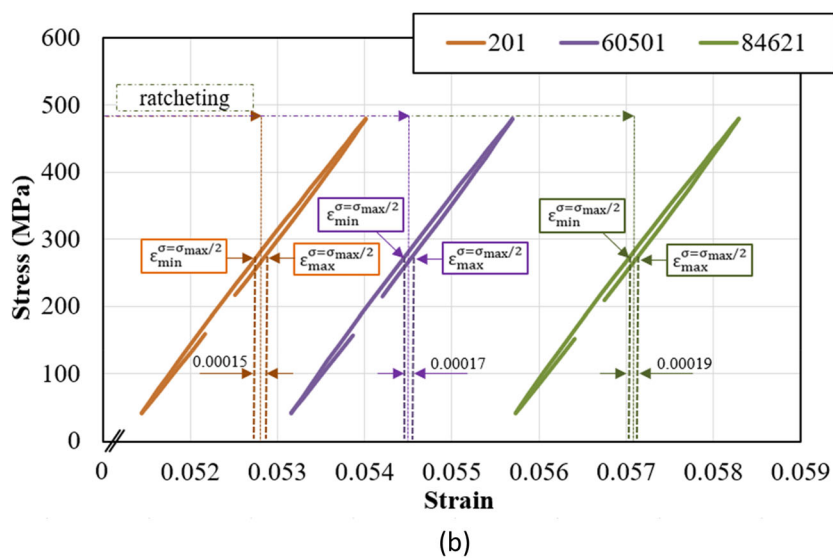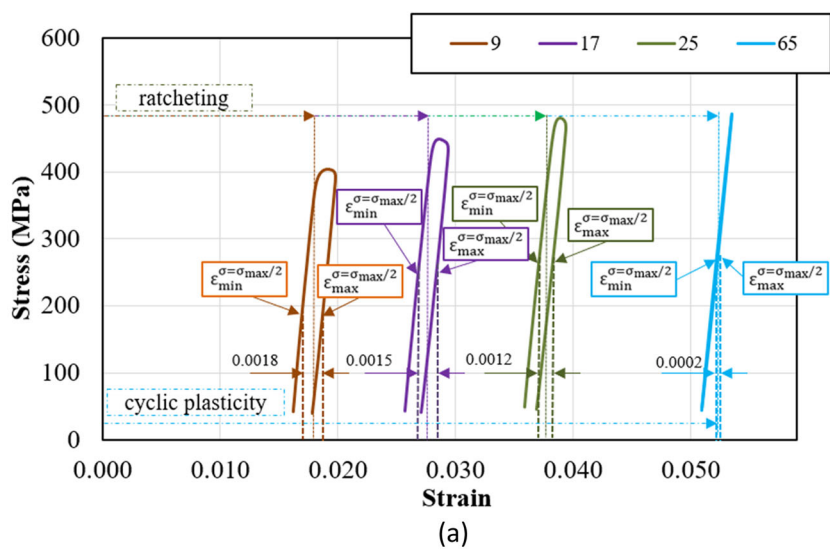
Fig. 8 Fatigue damage development of 13HMF steel for a stress of **a** 380 MPa; and **b** 500 MPa expressed by fatigue damage parameter D and fatigue damage measure variations as a function of a number of cycles supported by DIC measurements
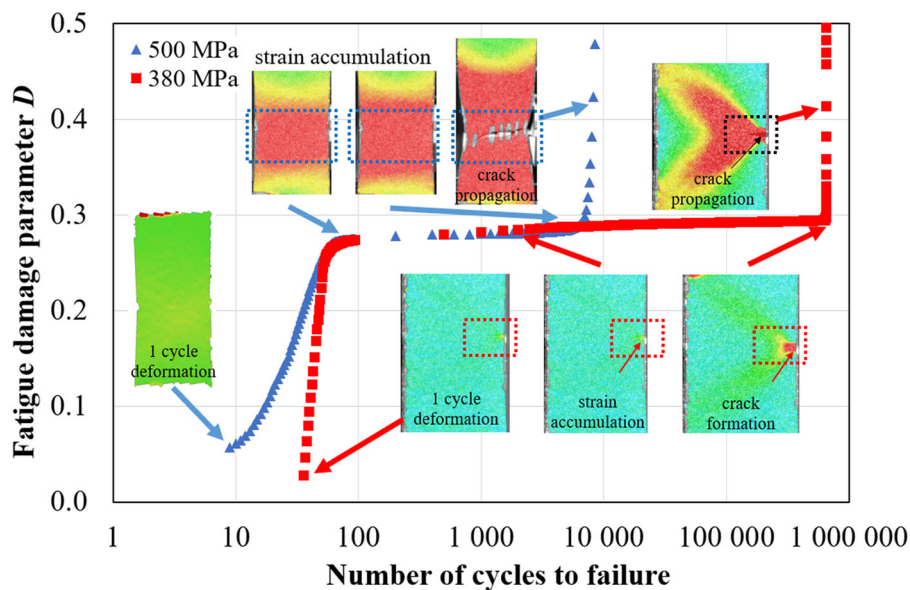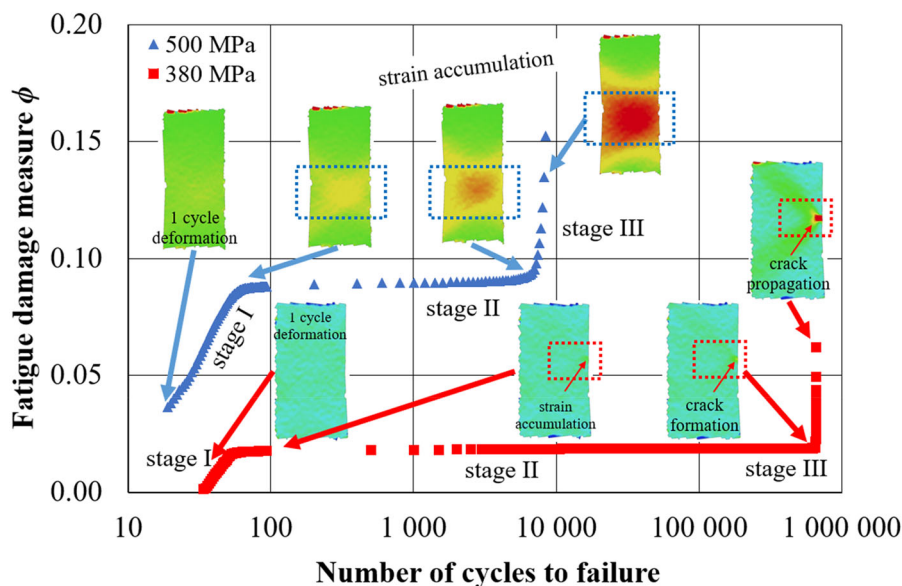
fatigue damage development. Since DIC maps could be registered for a particular fatigue cycle, they might be accurately allocated to the specific stage of deformation to effectively monitor material deformation. It was concluded that the correlation between DIC and damage parameter approach can be more effective than the conventional S–N curve approach in detailed description and understanding of the degradation process dynamics.

4 Conclusions

Fatigue damage development of 13HMF steel was effectively studied in the wide range of stress ranging from 320 to 500 MPa through a combined approach including the analytical determination of fatigue damage parameter D and the fatigue damage measure ϕ in subsequent cycles with the experimental DIC technique. The proposed methodology

Fig. 9 Selected strain profiles registered during DIC measurements for the specimens subjected to fatigue testing at stress equal to **a** 380 MPa; and **b** 500 MPa
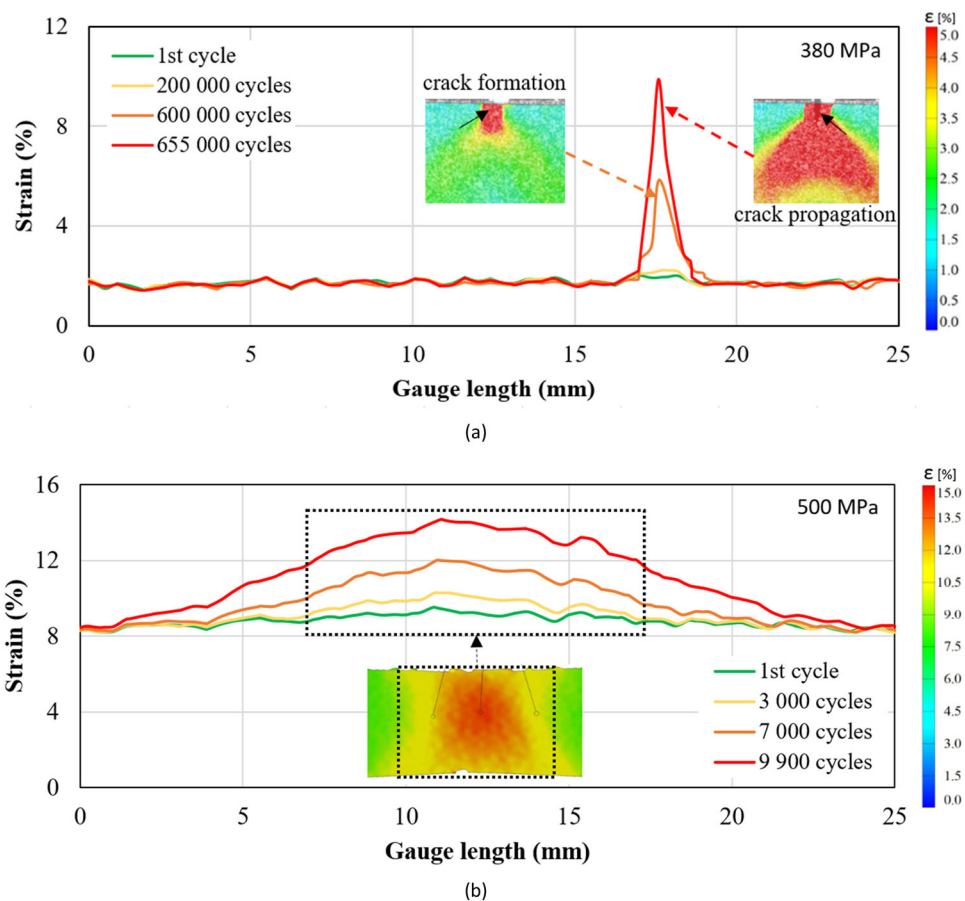
exposed the dynamics of damage within the first 100 cycles. Additionally, the DIC measurements enabled to localise the potential fracture area within the same number of cycles. The mutual validation of both attempts presented their great applicability in monitoring the fatigue damage development of power engineering steels.

Declarations

Conflicts of interest The author declares no conflict of interest.

Human and animal rights No animal or human subjects were used in this research.

References

1. Sroka M, Zieliński A, Dziuba-Kałuża M, Kremzer M, Macek M, Jasiński A. Assessment of the residual life of steam pipeline material beyond the computational working time. Metals. 2017;7(82):1–12.
2. Sroka M, Zieliński A, Mikuła J. The service life of the repair welded joint of Cr-Mo / Cr-Mo-V. Arch Metall Mater. 2016;61(3):1315–20.
3. Liu J, Hao XJ, Zhou L, Strangwood M, Davis CL, Peyton AJ. Measurement of microstructure changes in 9Cr–1Mo and 2.25Cr–1Mo steels using an electromagnetic sensor. Scripta Mater. 2012;66(6):367–70.

4. McEnteggart I. Extensometers. In: Sharpe W, editor. Springer Handbook of Experimental Solid Mechanics. Boston: Springer Handbooks; 208.

5. Mohanty JR, Verma BB, Ray PK. Prediction of fatigue crack growth and residual life using an exponential model: Part I (constant amplitude loading). Int J Fatigue. 2009;31(3):418–24.

6. Akramin MRM, Marizi MS, Husnain MNM, Shamil SM. Analysis of surface crack using various crack growth models. J Phys: Conf Ser. 2020;1529:1–6.

7. Bashiri AH, Alshoaibi AM. Adaptive finite element prediction of fatigue life and crack path in 2D structural components. Metals. 2020;10(10):1–20.

8. Nowell D, Paynter RJH, De Matos PFP. Optical methods for measurement of fatigue crack closure: moiré interferometry and digital image correlation. Fatigue Fract Eng Mater Struct. 2010;33:778–90.

9. Nelson DV. Residual stress determination using full-field optical methods. J Phys: Photonics. 2021;3:1–28.

10. Sieberer S, Viehböck EG, Schagerl M. Optical stress concentration and stress gradient monitoring during elasto-plastic fatigue tests with Digital Image Correlation. Mater Today: Proc. 2022;62(5):2543–8.

11. Risbet M, Feissel P, Roland T, Brancherie D, Roelandt JM. Digital Image Correlation technique: application to early fatigue damage detection in stainless steel. Procedia Eng. 2010;2:2219–27.

12. Qvale P, Zarandi EP, Ås SK, Skallerud BH. Digital image correlation for continuous mapping of fatigue crack initiation sites on corroded surface from offshore mooring chain. Int J Fatigue. 2021;151:1–12.

13. Vanlanduit S, Vanherzeele J, Longo R, Guillaume P. A digital image correlation method for fatigue test experiments. Opt Lasers Eng. 2009;47:371–8.

14. Niendorf T, Dadda J, Canadinc D, Maier HJ, Karaman I. Monitoring the fatigue-induced damage evolution in ultrafine-grained interstitial-free steel utilizing digital image correlation. Mater Sci Eng, A. 2009;517:225–34.

15. El Bartali A, Aubin V, Degallaix S. Fatigue damage analysis in a duplex stainless steel by digital image correlation technique. Fatigue Fract Eng Mater Struct. 2008;3:137–51.

16. Koster M, Kenel C, Lee WJ, Leinenbach C. Digital image correlation for the characterization of fatigue damage evolution in brazed steel joints. Procedia Mater Sci. 2014;3:1117–22.

17. Tanvir F, Sattar T, Mba D, Edwards G, Eren E, Lage Y. Identification of fatigue damage evolution in 316L stainless steel using acoustic emission and digital image correlation. MATEC Web of Conf. 2018;165:1–8.

18. Polish Standards PN-75/H-84024 – Steels for pipes – Grades.

19. Polish Standards PN10216–2: 2004 - Steel tubes for pressure purposes - Technical delivery conditions - Part 2: Non-alloy and alloy steel tubes with specified elevated temperature properties.

20. Boardman B. Fatigue Resistance of Steels. ASM Handbook, Volume 1: Properties and Selection: Irons, Steels, and High-Performance Alloys. ASM International; 1990;673–88

21. Hoeppner DW. Cyclic Loading and Cyclic Stress. In: Wang QJ, Chung YW, editors. Encyclopedia of Tribology. Boston: Springer; 2013.

22. Dhua SK, Ray A, Sen SK. Influence of nonmetallic inclusion characteristics on the mechanical properties of rail steel. J Mater Eng Perform. 2000;9:700–9.

23. Lin S, Wang D, Li C, Liu X, Di X, Jiang Y. Effect of cyclic plastic deformation on microstructure and mechanical properties of weld metals used for reel-lay pipeline steels. Mater Sci Eng, A. 2018;737:77–84.

24. Kopec M, Kukla D, Brodecki A, Kowalewski ZL. Effect of high temperature exposure on the fatigue damage development of X10CrMoVNb9-1 steel for power plant pipes. Int J Press Vessels Pip. 2021;189:1–16.

25. Srivatsan S, Sudarshan TS. Mechanisms of fatigue crack initiation in metals: role of aqueous environments. J Mater Sci. 1988;23:1521–33.

26. Wei X, Zhang C, Han S, Jia Z, Wang Ch, Xu W. High cycle fatigue S-N curve prediction of steels based on transfer learning guided long short term memory network. Int J Fatigue. 2022;163:1–10.

27. Moćko W, Grzywna P, Kowalewski ZL, Radziejewska J. An influence of cyclic loading on the form of constitutive relationship for DP500 steel. Mater Des. 2016;103:183–93.

28. León-Cázares FD, Monni F, Jackson T, Galindo-Nava EI, Rae CMF. Stress response and microstructural evolution of nickel-based superalloyys during low cycle fatigue: physics-based modelling of cyclic hardening and softening. Int J Plast. 2020;128:1–22.

29. Pandkar AS, Arakere N, Subhash G. Microstructure-sensitive accumulation of plastic strain due to ratcheting in bearing steels subject to rolling contact fatigue. Int J Fatigue. 2014;63:191–202.

30. Kukla D, Kowalewski ZL, Grzywna P, Kubiak K. Assessment of fatigue damage development in power engineering steel by local strain analysis. Kovove Mater-Metal Mater. 2014;52(5):269–77.